



ELSEVIER

Available online at www.sciencedirect.com

SCIENCE @ DIRECT®

Nuclear Instruments and Methods in Physics Research A 528 (2004) 139–145

NUCLEAR
INSTRUMENTS
& METHODS
IN PHYSICS
RESEARCH
Section A

www.elsevier.com/locate/nima

Study of partial-waveguide rf-linac FELs for intense THz-pulse generation

M. Tecimer^{a,*}, D. Oepts^b, R. Wuensch^c, A. Gover^a

^aPhysical Electronics, Tel Aviv University, 69978 Ramat Aviv, Tel-Aviv, Israel

^bFELIX-FOM, Rijnhuizen, 3430 BE Nieuwegein, The Netherlands

^cFZR, 1314 Dresden, Germany

Abstract

In this paper, we present a time-domain analysis of a short pulse partial-waveguide FEL oscillator employing toroidal mirrors and a hole outcoupling. The use of toroidal mirrors with optimized radius of curvatures helps to reduce cavity losses arising from the mismatch of the free space propagating optical field into a waveguided one. We introduce semi-analytical expressions for the calculation of the scattering matrix elements describing the loss and mode coupling mechanism as well as the amount of the extracted power from the cavity. The formulation is implemented in a time-domain FEL code based on modal expansion approach. The described model is applied to a partial-waveguide FEL system and simulation results are compared with measurements.

© 2004 Elsevier B.V. All rights reserved.

PACS: 41.60.Cr

Keywords: Free electron laser; Partial waveguide FEL; THz-pulse generation

1. Introduction

THz technology is being increasingly adopted in a wide variety of applications. The quest for tunable, coherent radiation sources in the THz region of the electromagnetic spectrum (~ 0.1 – 10 THz) stimulate further developments and research activities in this area. Owing to the increased availability, compactness and conveni-

ence in use, many of the applications utilize short pulse, broad-band THz-sources based on conventional laser technology. The available output power in those systems remain however low. In contrast, radiation sources based on accelerated electron devices, such as the (superconducting) rf-linac FEL systems can meet the needs of relatively narrow band, high-power (peak and average) coherent THz radiation offering a wide range of tunability over this spectrum. Due to the large diffraction losses inherent in this spectral region, the operation of rf-linac driven FELs often leads to the use of partial-waveguide resonators [1]. In

*Corresponding author.

E-mail addresses: tecimer@post.tau.ac.il, mtecimer@hawaii.edu (M. Tecimer).

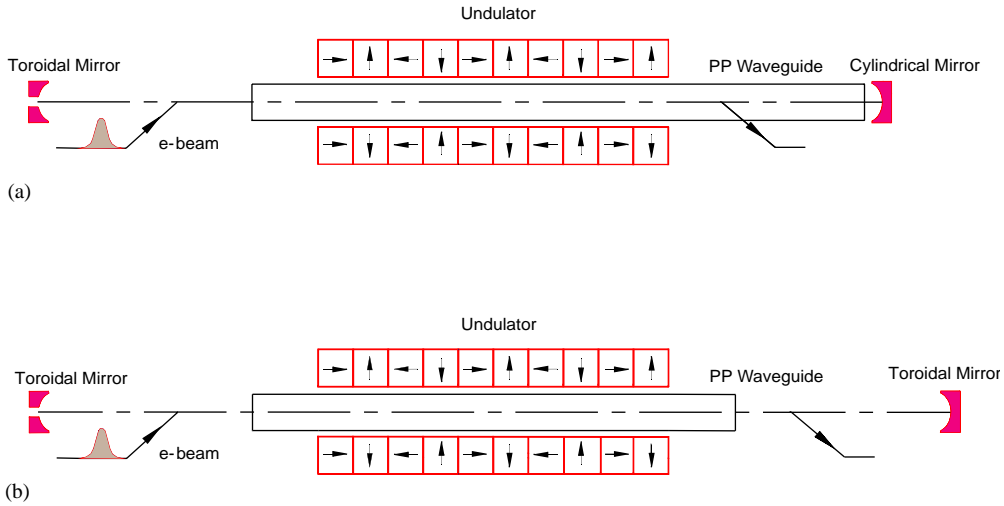


Fig. 1. Illustration of partial-waveguide resonator geometries employed in rf-linac FELs. (a) FELIX-FEL1's cavity utilizing a combination of a cylindrical and a toroidal mirror, (b) CLIO's two-sided partial-waveguide cavity.

Fig. 1a and b, two types of partial waveguide geometries are shown that are common in use. The resonator configuration shown in Fig. 1a has been realized in FELIX's FEL1 that is serving as a powerful, tunable THz-radiation source covering a spectrum range from ~ 30 to $250 \mu\text{m}$. The geometry shown in Fig. 1b has been implemented in CLIO's rf-linac FEL extending its wavelength range up to $120 \mu\text{m}$. Other rf-linac FEL systems such as FELICE ($\lambda \approx 3\text{--}100 \mu\text{m}$) and (superconducting) FZR-U90 ($\lambda \approx 30\text{--}150 \mu\text{m}$) will adopt a partial waveguide cavity design in order to reduce the diffraction losses and at the same time to achieve an increase in the filling factor when operating in the long wavelength region above $\sim 30 \mu\text{m}$ compared to an open resonator.

In this paper, an overview of the physical model presented that is implemented into the (partial-) waveguide FEL code "wgfel". As in the "Elixir" code on which the "wgfel" bases [2], the longitudinal motion is calculated for each macroparticle separately whereas the transverse motion is accounted for by the beam envelope equations. Finite pulse effects related to the slippage and cavity desynchronization are modeled taking into account the waveguide dispersion for each of the hybrid waveguide modes. To model losses and

mode-coupling effects due to the partial waveguiding a scattering matrix method is implemented into the oscillator simulation code which maps the amplitudes of the outgoing transverse modes from the waveguide aperture to the ones reflected and coupled back into it [3].

To verify the validity of the model employed, simulation results are compared with the experimental data obtained at the FELIX-FEL1.

2. Theoretical description of the model

In the following the field equation that governs the FEL dynamics in a (partially) waveguided resonator is presented. The normalized radiation vector potential A_r^- is expressed by the superposition of the cold cavity eigenmodes:

$$\vec{A}_r^-(\vec{x}_\perp, z, t) = \frac{e}{m_e c} \sum_{m,n} u_{mn}(z, t) \psi_{mn}(\vec{x}_\perp, z) \times \exp[i(k_{zn}z - \omega t)] \hat{e}_x. \quad (1)$$

In Eq. (1), $u_{mn}(z, t)$ is a time- and space-dependent complex envelope of a modulated wave train with carrier frequency ω and axial wave number k_z . The relation between ω and k_z is established by

the waveguide dispersion equation. The transverse profile of the optical field is defined by the transverse modes ψ_{mn} which are excited in a parallel plate waveguide (PPW) resonator [4]. Adopting slowly varying amplitude and phase approximation second-order inhomogeneous wave equation simplifies into

$$\partial_z u_{mn}(z, z') = \frac{j f_B \mathbf{F} A_{u0} \omega_p^2}{2k_{zn}} \frac{\omega_p^2}{c^2} \zeta_{mn}(z, \bar{z}) \frac{\chi(z, \bar{z})}{N_{\bar{z}}(z, \bar{z})} \times \sum_j^{N_{\bar{z}}(z, \bar{z})} e^{-i\theta_{jn}(z, \bar{z})} \quad (2)$$

where θ_{jn} is the ponderomotive phase with regard to n th mode. Eq. (2) results from transformations $z' = z - v_g t$ carried out for the radiation pulse longitudinal coordinate and $\bar{z} = z - v_z t$ for the electron beam pulse longitudinal coordinate. The longitudinal distribution of the particles is represented by the dimensionless function $\chi(z, \bar{z}) = N_{\bar{z}}(z, \bar{z})/n_0 \pi r_b^2 A$ [5,6]. In Eq. (2), F is the filling factor. ζ_{mn} results from averaging the source term over the transverse Gaussian density profile of the electron beam. It can be expressed by

$$\zeta_{mn}(z, \bar{z}) = \frac{\sqrt{1/\mu\varepsilon}}{8\sigma_x(z)\sigma_y(z)} \exp(\xi) \operatorname{erf}(\sqrt{\mu}X_0) \times \{ \exp(\theta^2/4\varepsilon)[\operatorname{erf}(\kappa_+) + \operatorname{erf}(\kappa_-)] + \exp(\theta^{*2}/4\varepsilon)[\operatorname{erf}^*(\kappa_+) + \operatorname{erf}^*(\kappa_-)] \} \quad (3)$$

with the following definition of the parameters:

$$\begin{aligned} X_0 &= 5\sigma_{x0}^2, & Y_0 &= 5\sigma_{y0}^2, & \xi &= -\frac{i}{2} \tan^{-1}(z/z_R) \\ \mu &= 1/w^2(z) - ik_{zn}/2R(z) + 1/2\sigma_x^2(z) \\ \varepsilon &= 1/2\sigma_y^2(z), & \nu &= (2n+1)\pi/g, & n &= 1, 3, 5, \dots \\ \theta &= k_u + iv, & \kappa_{\pm} &= \sqrt{\varepsilon}Y_0 \pm \theta/2\sqrt{\varepsilon} \end{aligned} \quad (4)$$

where σ_{x0} and σ_{y0} denote the rms beam waist in the transverse dimensions. $\sigma_x(z) = (\langle x^2 \rangle)^{1/2}$ and $\sigma_y(z) = (\langle y^2 \rangle)^{1/2}$ are the rms transverse dimensions of the beam that are defined by the solution of the beam envelope equations in terms of the longitudinal position “ z ” [2].

2.1. Slippage and feedback loop in a short pulse (partial-) waveguide oscillator

Due to the waveguide dispersion, slippage effects in short pulse waveguide FELs exhibit differences in comparison with open resonator FELs. The slippage length L_{sp} for the resonant radiation wavelength λ_r is defined as

$$\begin{aligned} L_{sp} &= [(\beta_g/\beta_z) - 1]N\lambda_u \\ &= N\lambda_r[1 - (k_{\perp}/\beta_z\gamma_z k_u)^2]^{1/2} \end{aligned} \quad (5)$$

where N and $k_{\perp n}$ are, respectively, the number of the undulator periods and the cutoff wave number of the m th transverse mode. L_{sp} is mode dependent since each transverse mode overtakes the electron beam with a different group velocity.

The boundary conditions imposed by the resonator mirrors are included into the feedback of the radiation field. For the transverse modes the feedback is described by

$$\begin{aligned} u_{m'n''}^{(p+1)}(z=0, t) &= R^{(1)}R^{(2)} \times \sum_{m', n'} \sum_{m, n} P_{m''n''m'n'}^{(1)} P_{m'n'mm}^{(2)} \\ &\times e^{i\Phi_{m''n''}(\omega)} u_{mn}^{(p)}(L_u, t - t_r) \end{aligned} \quad (6)$$

where $u_{mn}^{(p)}(L_u, t')$ denotes the complex amplitude of the m th mode at the exit of the interaction region and the suffix “ p ” the number of passes. $t_r = 2(L_{wg}/v_{gn} + L_f/c)$ is the cavity roundtrip time, L_{wg} and L_f correspond to the waveguided and free space parts of the resonator, respectively. The cavity roundtrip phase shift is given by

$$\Phi_{m''n''}(\omega) = 2[k_{zn}(\omega)L_{wg} + k_s L_f] + \Delta\Phi_G \quad (7)$$

including the Gouy phase shift $\Delta\Phi_G$ of the hybrid mode. The resonance frequency condition of the cavity is satisfied when $\Phi_{m''n''}(\omega)$ is a multiple of 2π . The intermode scattering between the reflected modes due to the partial waveguiding and the outcoupling hole are expressed by the scattering matrices $P^{(j)}$ ($j = 1, 2$) where the suffix “ j ” signifies upstream and downstream mirrors. $R^{(j)}$ denotes the amplitude reflection coefficient accounting for the ohmic losses on the mirror surfaces.

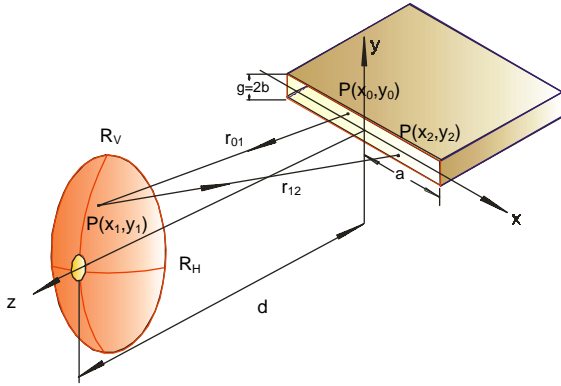


Fig. 2. After interacting with a short electron pulse, the parallel plate waveguide modes Ψ_{mn} propagate in free space to a toroidal mirror.

2.2. Partial PPW resonator

In the hole outcoupled partial-waveguide resonator with toroidal mirrors, cavity loss and mode coupling have been determined by calculating the scattering matrix elements. Here, we evaluate Huygens–Fresnel diffraction integrals describing the free space propagation of the optical field at the exit of a overmoded waveguide to finite size toroidal mirrors ($R_V \neq R_H$), outcoupling through a hole and matching of the back-reflected field into the waveguide aperture (Fig. 2). In the Fresnel approximation, the diffraction integral describing the propagation of the mode $\psi_{mn}(\vec{x}, z)$ to the toroidal mirror is given by

$$E_{(mn)}(\vec{x}_1, d) = \left(\frac{1}{i\lambda d N_{mn}} \right) A_{01} \times \int_{-b}^b \int_{-a}^a \exp(-ik((x_1 x_0 + y_1 y_0)/d)) \times \exp(ik(x_0^2 + y_0^2)/2d) \psi_m(x_0, z_0) \times \psi_n(y_0) dx_0 dy_0 \quad (8)$$

where a and b are the half-width and height of the waveguide aperture, $A_{01} = \exp(ikd) \exp(ikx_1^2(1 - d/R_H)/2d) \exp(iky_1^2(1 - d/R_V)/2d)$ and R_H and R_V are the horizontal and vertical mirror radius of curvatures, respectively (Fig. 2). The integral in

Eq. (8) can be expressed by

$$E_{mn}(\vec{x}_1, d) = \left(\frac{1}{i\lambda d N_{mn}} \right) A_{01} \frac{\sqrt{\pi}\xi(1+i)}{8\sqrt{2\beta\mu}} \exp\left(-\frac{k^2}{4\mu d}\right) \times \left\{ \operatorname{erf}\left(\sqrt{\mu}a + \frac{ikx_1}{2d\sqrt{\mu}}\right) + \operatorname{erf}\left(\sqrt{\mu}a - \frac{ikx_1}{2d\sqrt{\mu}}\right) \right\} \times \left\{ \exp\left(-\frac{i\pi f_{y(-)}^2}{\beta}\right) [\operatorname{erf}(\Theta\Gamma_1) + \operatorname{erf}(\Theta\Gamma_2)] + \exp\left(-\frac{i\pi f_{y(+)}^2}{\beta}\right) [\operatorname{erf}(\Theta\Gamma_3) + \operatorname{erf}(\Theta\Gamma_4)] \right\} \quad (9)$$

where we define $\Theta = \sqrt{\pi\beta}/2(1+i)$, $\beta = 1/\lambda d$, $\alpha = (n+1/2)/g$, $\gamma = \alpha/\beta$, $f_{y(\pm)} = \beta y_1 \pm \alpha$, $\Gamma_{1,2} = b \mp (y_1 - \gamma)$, $\Gamma_{3,4} = b \mp (y_1 + \gamma)$, and the normalization factor $N_{mn} = (2^m m! \sqrt{\pi/8wg(z)g})^{1/2}$. Eq. (9) allows to calculate the outcoupled radiation power through the hole at any z' within the pulse:

$$P_{\text{out}}(d, z') = \frac{kk_{zn}}{2Z_0} (m_e c^2 / e)^2 \times \sum_{mn} \sum_{m'n'} \int_{-h_r}^{h_r} dy_1 \int_{-\sqrt{1-y^2}}^{\sqrt{1-y^2}} u_{mn}(L_{wg}, z') u_{m'n'}^*(L_{wg}, z') \times E_{mn}(\vec{x}_1, d, z') E_{m'n'}^*(\vec{x}_1, d, z') dx_1 \quad (10)$$

$u_{mn}(L_{wg}, z')$ being the complex field amplitude of the mode “ mn ” at the exit of the waveguide aperture. The complex field amplitude of the back reflected field at the waveguide aperture is defined by

$$E_{mn}(\vec{x}_2, 2d) = \left(\frac{1}{i\lambda d N_{mn}} \right) \exp(ikd) \exp(ik(x_2^2 + y_2^2)/2d) \times \left[\int_{-R_y}^{R_y} dy_1 \int_{-R_x}^{R_x} \frac{\sqrt{1-y_1^2/R_y^2}}{\sqrt{1-y_1^2/R_x^2}} \exp(-ik((x_2 x_1 + y_2 y_1)/d)) \times \exp(ik(x_1^2 + y_1^2)/2d) E_{mn}(\vec{x}_1, d) dx_1 \right]$$

$$\begin{aligned}
 & - \int_{-h_r}^{h_r} dy'_1 \int_{-\sqrt{h_r^2 - y'^2_1}}^{\sqrt{h_r^2 - y'^2_1}} \exp(-ik((x_2 x'_1 + y_2 y'_1)/d) \\
 & \times \exp(ik(x'^2_1 + y'^2_1)/2d) E_{mn}(\vec{x}'_1, d) dx'_1 \Big]. \quad (11)
 \end{aligned}$$

In Eq. (11), limits of the first integration define toroidal mirror’s transverse extension and h_r is the outcoupling hole radius. The projection of the back reflected field $E_{m'n'}(\vec{x}^-_2, 2d)$ into the m th PPW mode is defined by

$$P_{m'n'mn} = \frac{1}{N_{mn}} \int_{-b}^b \int_{-a}^a E_{m'n'}(\vec{x}_2, 2d) \psi_{mn}^*(\vec{x}_2, 2d) d^2 \vec{x}_2. \quad (12)$$

$P_{m'n'mn}$ being the scattering matrix element. The complex field amplitude u_{mn} at the exit of the PPW following the interaction section is related to the backreflected $u_{m'n'}$ containing the cavity loss by

$$u_{m'n'} = \sum_{m,n} P_{m'n'mn}^T u_{mn}. \quad (13)$$

3. Numerical results

Experimental data obtained at the partial waveguide THz-FEL in FELIX by the cavity ring down measurements, output pulse energies and pulse shape measurements is used to verify the validity of the model employed. An overall system

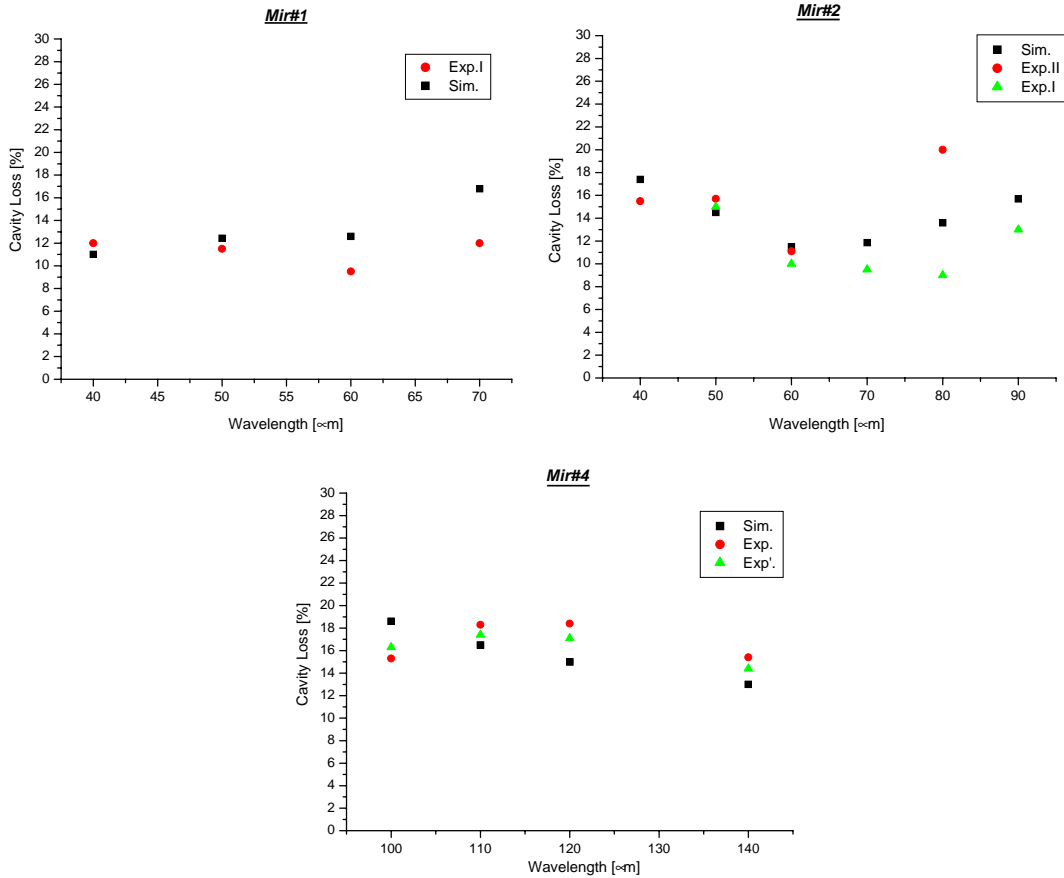


Fig. 3. Cavity roundtrip losses for the wavelength region 40–140 μm using various mirrors at FELIX’s partial-waveguide resonator. The loss data is deduced from the cavity ring-down measurements.

description of FEL1 can be found in Ref. [1]. Fig. 3 shows the cavity losses deduced from the decay rate of the extracted radiation power versus radiation wavelength for individual toroidal mirrors. The measurements include two sets of independently taken experimental data. The simulated cavity loss L_{mn} due to the outcoupling hole, finite size toroidal mirror, clipping off at the waveguide aperture and mode-conversion is given by $L_{mn} = 1 - |P_{m'n'mm}|$. In the simulations, combination of TE_{01} , TE_{03} , TE_{05} composes the startup field's transverse mode pattern. The scattering from TE_{01} mode into higher-order modes leads merely to a loss channel of energy since the latter are not sustained by the cavity nor by the gain medium.

The presented numerical results rely on the assumption that the electron injection into the undulator occurs without inducing beam-misalignments with respect to the optical axis of a perfectly aligned resonator. Although they mimic with reasonable agreement the measured wavelength dependent behavior of cavity losses shown in Fig. 3, it is also apparent from the data obtained for mirrors #1–#2 that some of the measured cavity losses happen to be smaller than the computed ones, particularly when the investigated wavelength increases. The latter might be originating from electron beam/resonator-axis misalignment by matching and subsequent steering of the beam through the undulator as the gap is changed to vary the undulator parameter K_{rms} . In the lateral, where the waveguide width is seven times larger than the height, the excitation of the next order free space mode and its coupling to a slightly off-axis steered beam in the same plane is facilitated. In analogy to the cases reported in Refs. [7,8], the maximum intensity of the excited asymmetrical field pattern does not coincide with the hole aperture axis, leading to a reduction in the outcoupling fraction, consequently also to a lower total cavity loss. In Fig. 4, extracted micropulse energies obtained at various toroidal mirror geometries and wavelengths in the region between 40 and 140 μm are compared with the simulated ones. Here, the employed cavity detuning has been optimized to obtain the maximum outcoupled pulse energies. In Fig. 5, detected time structure of

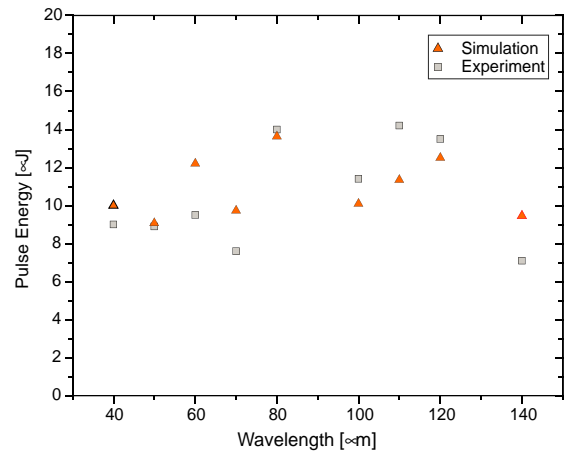


Fig. 4. The outcoupled micropulse energies versus wavelength. The beam energy (14–21 MeV) and the undulator parameter (~ 0.8 –1.5) are varied to adjust for the wavelength.

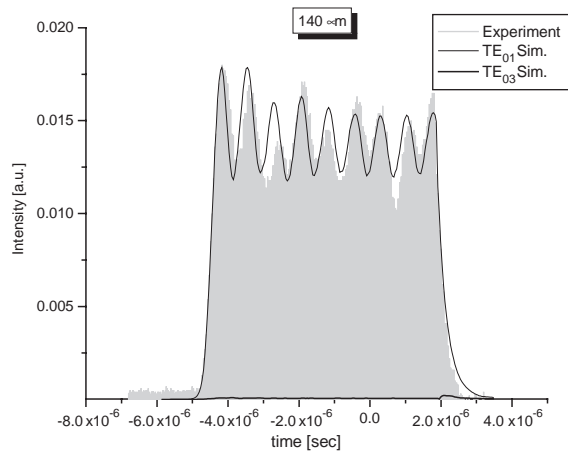


Fig. 5. Detector signal of a macropulse at 140 μm , outcoupled from mirror#4. Simulated macropulse intensity is normalized to the first peak (at saturation) of the measured signal.

a $\sim 8 \mu\text{s}$ long macropulse at 140 μm , coupled out from toroidal mirror #4, is compared with the simulated one. Note that, here, the measured output power is scaled to arbitrary units since the detector used in this measurement (P5-01, Molectron) was not calibrated for absolute power measurements. The contribution of TE_{03} mode to the total radiated intracavity power remains according to the simulations around noise level of the detected signal. The measured macropulse

shape exhibits $\sim 8\frac{1}{2}$ limit cycle oscillations for a cavity desynchronization set to -0.8 to -0.9λ . The ‘wgfel’ code uses -1.2λ to fit the simulated pulse shape to the measured one.

4. Conclusion

The physical model presented in this paper provides a means to describe two important aspects of partially waveguided, short pulse FEL oscillators and the interplay between them during the radiation buildup process in multiple passes; short pulse effects in a dispersive medium, and the dynamics of mode-conversion/cavity losses due to abrupt transitions caused by various apertures used in the adopted resonator geometry. The described model is applied to the partial-waveguide THz-FEL in FELIX, making comparisons with the experimental results. Cavity losses and extracted pulse energies at various toroidal mirror

geometries and beam energy/undulator settings are presented. Discrepancies exist between the simulation results and the experimental observations in the cases where the axially symmetric simulation model cannot handle misaligned resonators and/or off-axis electron beams.

References

- [1] K.W. Berryman, T.I. Smith, Nucl. Instr. and Meth. A 318 (1992) 885; FELIX, <http://www.rijnh.nl>, Characteristics of Felix; L.Y. Lin, A.F.G. van der Meer, Rev. Sci. Instrum. 68 (1997) 4342.
- [2] G. van Werkhoven, et al., Phys. Rev. E 50 (1994) 4063.
- [3] M. Tecimer, Nucl. Instr. and Meth. A 483 (2002) 521.
- [4] L. Elias, J. Gallardo, Appl. Phys. B 31 (1983) 229.
- [5] R. Bonifacio, et al., Phys. Rev. A 44 (1991) 3441.
- [6] B.W.J. McNeil, Opt. Commun. 165 (1999) 65.
- [7] G.A. Barnett, et al., Nucl. Instr. and Meth. A 358 (1995) 311.
- [8] V.I. Zhulin, Nucl. Instr. and Meth. A 375 (1996) ABS 85.